with wire mesh (8 mm between wires), and 42 cm high. The water level was 1.6 cm above the level of the platform, which was placed in the middle of one quadrant (SE) of the pool, midway between wall and pool center. The water (21° ± 2°C) was made opaque by the addition of 7.2 kg of powdered low-fat milk. Tracking of mice was as described (*51*). A month before the actual experiment, the mice swam daily for 13 days (platform NW) in a smaller pool (60 cm), which accustomed them to mounting the platform. *Spatial navigation trials*: Mice (19 wild type, 21 GluR-A$^{-/-}$) were gently placed into the water at the edge of the pool at one of four start positions arbitrarily named N, S, E, and W. In a block of four trials all start positions were used in a semirandom order that differed every day. Finding the platform was defined as climbing onto it and staying for at least 5 s. Once on the platform, the mouse was allowed to stay for 30 s. For any mouse that failed to find the platform within 90 s, a latency of 90 s was recorded, and the mouse was placed on the platform. To ensure that the mouse did not use cues inside the pool, we rotated the pool daily and removed floating debris and feces before every trial. *Transfer trials*: On transfer trials the mice were placed onto the edge of the pool and allowed to swim with no platform present. The video system recorded the percentage of time spent in the various quadrants. The experimenter recorded from a video monitor the number of times the mouse crossed the previous position of the platform; crosses were defined by the head fully entering the square representing the platform position. *Transfer trial in the absence of visual cues*: To hide distal visual cues, we hung white curtains from the ceiling in a circle (2 m diameter around the pool).
31. A. Baude *et al.*, *Neuroscience* **69**, 1031 (1995); M. E. Rubio and R. J. Wenthold, *Neuron* **18**, 939 (1997).
32. R. A. Silver *et al.*, *J. Physiol.* (*London*) **493**, 167 (1996).
33. R. C. Malenka and R. A. Nicoll, *Neuron* **19**, 473 (1997).
34. We studied LTP in the lateral and medial perforant path synapses of dentate granule cells. In adult GluR-A$^{-/-}$ mice, the magnitude of LTP was about half that of wild type. In wild-type mice (n = 4) the values (±SEM) were 128% ± 11% (n = 10) and 132% ± 7% (n = 8) of the pretetanic amplitudes for the lateral and medial perforant path synapses, whereas GluR-A$^{-/-}$ mice (n = 5) showed 113% ± 4% (n = 10) and 118% ± 5% (n = 11) for the same two inputs. The data are not explained by a smaller proportion of mutant slices showing potentiation.
35. N. Meiri *et al.*, *Proc. Natl. Acad. Sci. U.S.A.* **95**, 15037 (1998); S. Schurmans *et al.*, *ibid.* **94**, 10415 (1997); M. Nosten-Bertrand *et al.*, *Nature* **379**, 826 (1996); Y. Y. Huang *et al.*, *Cell* **83,** 1211 (1995); S. Okabe *et al.*, *J. Neurosci.* **18**, 4177 (1998).
36. R. G. M. Morris and U. Frey, *Philos. Trans. R. Soc. London Ser. B* **352**, 1489 (1998).
37. M. Köhler, H.-C. Kornau, P. H. Seeburg, *J. Biol. Chem.* **269**, 17367 (1994).
38. D. Feldmeyer *et al.*, *Nature Neurosci.* **2**, 57 (1999).
39. A. Nagy, J. Rossant, R. Nagy, W. Abramow-Newerly, J. C. Roder, *Proc. Natl. Acad. Sci. U.S.A.* **90**, 8424 (1993).
40. H. Gu, Y.-R. Zou, K. Rajewsky, *Cell* **73**, 1155 (1993).
41. H. Markram *et al.*, *J. Physiol.* (*London*) **500**, 409 (1997).
42. W. Sather, S. Dieudonne, J. F. MacDonald, P. Ascher, *ibid.* **450**, 643 (1992).
43. P. Jonas, G. Major, B. Sakmann, *ibid.* **472**, 615 (1993).
44. R. Sprengel *et al.*, *Cell* **92**, 279 (1998).
45. K. D. Phend, R. J. Weinberg, A. Rustioni, *J. Histochem. Cytochem.* **40**, 1011 (1992).
46. M. Frotscher, *Microsc. Res. Tech.* **23**, 306 (1992).
47. F. Helmchen, K. Imoto, B. Sakmann, *Biophys. J.* **70**, 1069 (1996).
48. G. Grynkiewicz, M. Poenie, R. Y. Tsien, *J. Biol. Chem.* **260**, 3440 (1985).
49. W. Denk, J. H. Strickler, W. W. Webb, *Science* **248**, 73 (1990); H. J. Koester and B. Sakmann, *Proc. Natl. Acad. Sci. U.S.A.* **95**, 9596 (1998).
50. D. W. Saffen *et al.*, *Proc. Natl. Acad. Sci. U.S.A.* **85**, 7795 (1998).
51. P. H. Kelly and J. Malanowski, *Can. J. Physiol. Pharmacol.* **71**, 352 (1993).
52. K. Kask *et al.*, *Proc. Natl. Acad. Sci. U.S.A.* **95**, 13777 (1998). Membrane proteins of hippocampi were processed for immunoblot analysis with glutamate receptor 1 polyclonal antibody (Chemicon, Temecula, CA) at 0.5 to 1 μg/ml. After visualization by enhanced chemiluminescence (ECL, Amersham Corp.) blots were stripped and reprobed with glutamate receptor 2 polyclonal antibody at 1 μg/ml (T62-3B) (*18*) and with an NR1 monoclonal antibody (54.1) at 3 μg/ml.
53. Supported in part by the Volkswagen-Stiftung (R.S., P.H.S., B.S.), the Deutsche Forschungsgemeinschaft (P.H.S.), and Bristol-Myers Squibb (P.H.S.). We thank H. Gu for the plasmid pMC-Cre, A. Nagy for the R1 ES cell line, R. Morrison and J. R. Wenthold for providing antibodies, and M. Lang, A. Herold, S. Nestel, and B. Joch for technical assistance. D.Z. was the recipient of a postdoctoral fellowship from the Human Frontier Science Program.

3 March 1999; accepted 11 May 1999

Rapid Spine Delivery and Redistribution of AMPA Receptors After Synaptic NMDA Receptor Activation

Song-Hai Shi,[1] Yasunori Hayashi,[1] Ronald S. Petralia,[2] Shahid H. Zaman,[1] Robert J. Wenthold,[2] Karel Svoboda,[1] Roberto Malinow[1] *

To monitor changes in α-amino-3-hydroxy-5-methyl-4-isoxazole propionate (AMPA) receptor distribution in living neurons, the AMPA receptor subunit GluR1 was tagged with green fluorescent protein (GFP). This protein (GluR1-GFP) was functional and was transiently expressed in hippocampal CA1 neurons. In dendrites visualized with two-photon laser scanning microscopy or electron microscopy, most of the GluR1-GFP was intracellular, mimicking endogenous GluR1 distribution. Tetanic synaptic stimulation induced a rapid delivery of tagged receptors into dendritic spines as well as clusters in dendrites. These postsynaptic trafficking events required synaptic *N*-methyl-D-aspartate (NMDA) receptor activation and may contribute to the enhanced AMPA receptor–mediated transmission observed during long-term potentiation and activity-dependent synaptic maturation.

Excitatory synaptic transmission in the vertebrate central nervous system is mediated by activation of AMPA- and NMDA-type glutamate receptors. Repetitive synaptic activity transiently activates NMDA receptors and triggers long-lasting plasticity (*1*), expressed, at least in part, as an increase in AMPA receptor function (*2*, *3*). The molecular basis for activity-induced changes in AMPA receptor function is not known and may include changes in channel conductance (*4*), possibly after receptor phosphorylation (*5*), or delivery of AMPA receptors to synapses, as has been documented during development (*6*). We investigated if an increase in AMPA receptor number at synapses may occur rapidly during NMDA receptor–dependent synaptic plasticity.

AMPA receptors are oligomers formed by a combination of four different subunits, GluR1 to 4 (GluRA to D) (*7*). A substantial proportion of endogenous AMPA receptors in hippocampal neurons have the GluR1 subunit (*8*). We constructed a recombinant GluR1 tagged with green fluorescent protein (GFP) at the putative extracellular NH_2-terminus (GluR1-GFP; Fig. 1A) (*9*). This protein was expressed in human embryonic kidney (HEK) 293 cells; extracts showed a single band by protein immunoblotting of the expected molecular mass (Fig. 1B). Whole-cell recordings from GluR1-GFP–transfected HEK 293 cells showed inwardly rectifying responses to puffed agonist (Fig. 1C) (*7*). Cotransfection of GluR1-GFP with wild-type GluR2 yielded responses with no rectification (Fig. 1C), indicating effective hetero-oligomerization between GluR1-GFP and GluR2, as homomeric GluR2 can produce little current (*7*).

GluR1-GFP was introduced into neurons with Sindbis virus expression system (*10*, *11*). In hippocampal dissociated cultured neurons (Fig. 2) (*12*), GluR1-GFP showed distribution throughout the dendritic tree with expression levels in dendrites approximately three times that of endogenous GluR1 (*13*). Immunostaining for surface (Fig. 2D) (*14*)

[1]Cold Spring Harbor Laboratory, Cold Spring Harbor, NY 11724, USA. [2]Laboratory of Neurochemistry, National Institute on Deafness and Other Communication Disorders, National Institutes of Health, Bethesda, MD 20892–4162, USA.

*To whom correspondence should be addressed. E-mail: malinow@cshl.org

recombinant receptor displayed a punctate distribution that colocalized with surface labeling of endogenous GluR2 (Fig. 2D) as well as with a presynaptic marker (synapsin 1; Fig. 2D). Whole-cell responses to caged glutamate showed greater rectification in GluR1-GFP–expressing neurons, indicating functional delivery of homomeric GluR1-GFP to the surface (Fig. 2B) (*15*).

We next examined the distribution of GluR1-GFP in neurons of organotypic hippocampal slice cultures (*16*) because such a preparation can display robust long-term potentiation (LTP) (Fig. 3A). Two to 3 days after focal viral infection of the CA1 region (*17*), several hundred neurons showed GluR1-GFP expression (Fig. 3B) distributed throughout the apical and basal dendritic trees. To quantify the subcellular distribution of recombinant receptor in these slice cultures, we used postembedding immuno-gold electron microscopy with an antibody directed against GFP (*18*, *19*). We examined apical dendritic areas in infected regions (Fig. 3, E and F). Most of the labeling in dendrites was located intracellularly in the dendritic shaft (88%). The remainder was largely (9%) on the dendritic shaft surface, with little (2%) in spines, and only three grains (0.4%) were found at postsynaptic densities, sites of synaptic contact. This distribution pattern was in general similar to that of endogenous GluR1, detected with an antibody to GluR1 in comparable dendritic regions from (noninfected) postnatal day 10 brain tissue (Fig. 3F). Most of the endogenous GluR1 labeling in dendrites was also intracellular in the dendritic shaft (71%), with 20% on the dendritic shaft surface and 8% in surrounding spines [3% was in postsynaptic densities (PSD)] (*20*).

To monitor changes in the distribution of GluR1-GFP, we used time-lapse two-photon laser scanning microscopy (TPLSM) (*21*) and examined neurons in organotypic slices 2 to 3 days after infection. High-resolution optical stack images of dendritic regions revealed that the GluR1-GFP signal was fairly homogeneous (Fig. 3, B and C) along the dendrite and largely restricted from dendritic spines, consistent with the immuno-gold electron microscopic analysis (Fig. 3F) and in contrast to the distribution of plain GFP, which displayed numerous spines (Fig. 3D). To test the effect of synaptic activity on receptor distribution, we placed a small glass-stimulating electrode near (5 to 15 μm) a group of dendrites labeled with GluR1-GFP (*22*). In the absence of evoked activity, the GluR1-GFP distribution pattern was stable for hours with no signs of photodamage and little bleaching (see below; for example, Fig. 6A). However, delivery of a brief tetanic stimulus, which was sufficient to induce LTP in these slices (Fig. 3A), produced a rapid redistribution of GluR1-GFP (Figs. 4 to 6).

Two kinds of changes in GluR1-GFP distribution were detected after tetanic stimulation: delivery to spines and clustering in the dendritic shaft. Delivery of GluR1-GFP was measured in 38 spines from five experiments (Fig. 4). In about half of these spines (17 of 38), the amount of fluorescence at the corresponding location in images obtained before a tetanus was near background (*23*) (termed "empty" spines, Fig. 4A, arrow a), whereas in

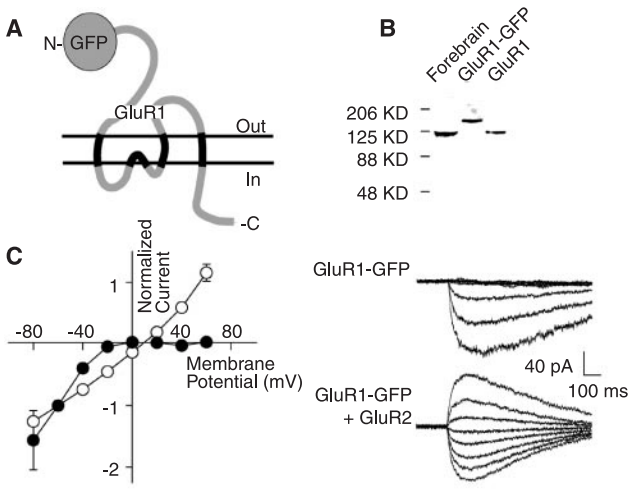

Fig. 1. Expression and functional analysis of GluR1 fused with GFP (GluR1-GFP). (**A**) Schematic drawing of expected transmembrane topology of GluR1-GFP. N, NH_2-terminus; C, COOH-terminus. (**B**) Protein immunoblotting of membrane fractions of rat forebrain and HEK cells transfected with GluR1-GFP or GluR1, probed with antibody to GluR1 COOH-terminus. The increase in molecular mass in GluR1-GFP is comparable with the molecular mass of GFP (27 kD). There was no other band detected at lower molecular mass. (**C**) (Left) Current-voltage plots of whole-cell responses from HEK 293 cells transfected with GluR1-GFP alone (●, $N = 3$) and with GluR1-GFP with GluR2 (○, $N = 3$). Responses are normalized to values at −60 mV. (Right) Representative responses at membrane potentials from −80 to +60 mV (20-mV steps). One millimolar kainic acid was puff applied in the presence of 100 μM cyclothiazide.

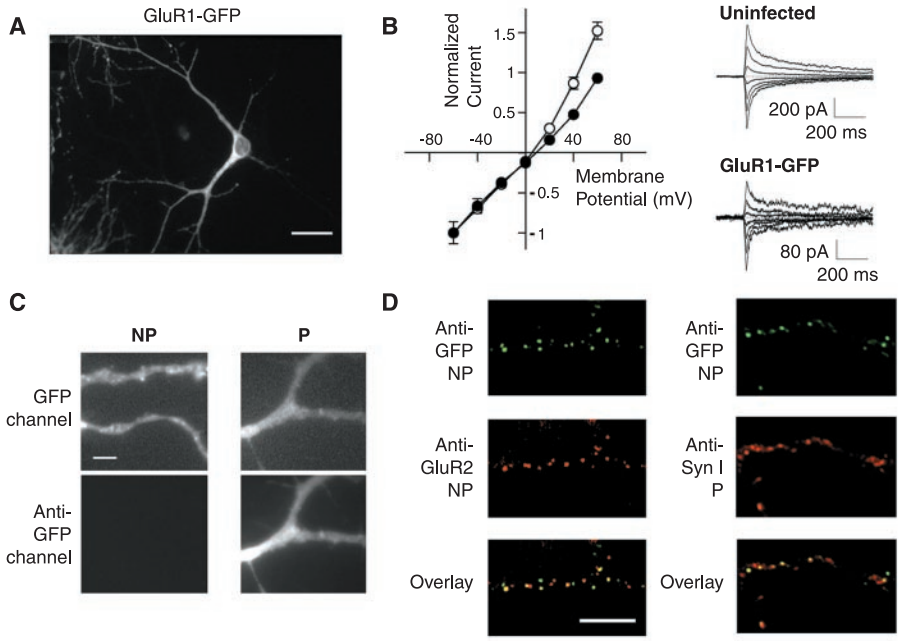

Fig. 2. Expression of GluR1-GFP in dissociated cultured hippocampal neurons is targeted to synapses. (**A**) Neuron 1 day after infection expressing GluR1-GFP. Scale bar, 30 μm. (**B**) Whole-cell responses to uncaged glutamate (10 ms, 40 μM CNB-glutamate). (Left) Current-voltage relations plotted, normalized to values at −60 mV. ●, infected cell ($n = 8$); ○, uninfected cell ($n = 8$). (Right) Responses from uninfected (top) and infected (bottom) neuron at different holding potentials (−60 mV to +60 mV, 20-mV steps). (**C**) Dissociated cultured neurons expressing plain GFP were fixed in nonpermeabilizing (NP) or permeabilizing (P) conditions (*14*), stained with antibody to GFP, and imaged with filters for GFP (top) or antibody to GFP (Texas Red) (bottom). The same gray scale was used on all images. Scale bar, 2 μm. (**D**) Surface expression of GluR1-GFP. Immunostaining with antibodies to GFP (polyclonal for double staining with GluR2 and monoclonal for synapsin I, both at 1:100; Clontech) under nonpermeabilized conditions reveals punctate pattern of expression. This punctate pattern colocalizes with endogenous GluR2 (left) detected with antibody against extracellular domain of GluR2 (10 μg/ml; Chemicon International) and synapsin I (Syn I) (1:100) (immunostained after permeabilizing conditions) (right). Scale bar, 5 μm.

the remaining 21 of 38 spines (termed "active" spines, Fig. 4A, arrow b), there was a detectable amount of GluR1-GFP before tetanus. The intensity distribution of these analyzed spines is shown in Fig. 4, B and C. The GluR1-GFP signal at "empty" spines increased from 200 ± 43 AU to 1737 ± 235 AU [measured in arbitrary fluorescence units (AU); mean ± SD, $N = 17$] after a tetanic stimulus. At "active" spines, the increase was from 1023 ± 101 AU to 2210 ± 235 AU (mean ± SD, $N = 21$). Such increases in GluR1-GFP signals at spines were never observed in the absence of tetanic stimulation (*24*).

In addition to spine delivery, tetanic stimulation produced clustering of GluR1-GFP in the dendritic shaft. The clustered receptor

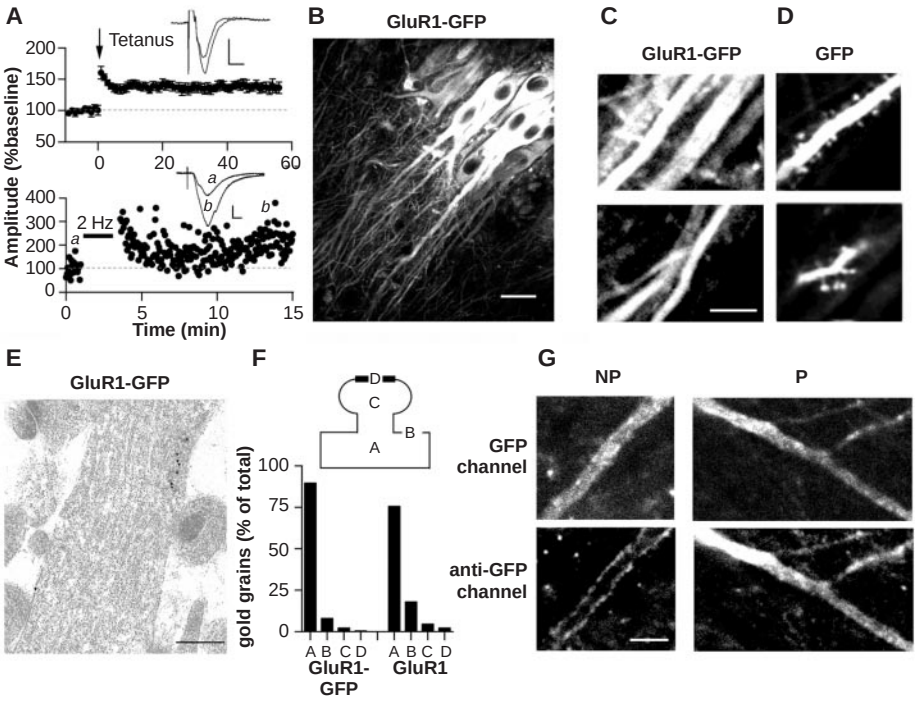

Fig. 3. GluR1-GFP expression in organotypic hippocampal slice culture is primarily intracellular. (**A**) Organotypic slice culture displays LTP in CA1. (Top) Plot of field excitatory postsynaptic potentials recorded in CA1 region of organotypic slice (mean ± SEM, $N = 5$; tetanus: time = 0). (Bottom) Whole-cell recording of synaptic responses from neuron expressing GluR1-GFP. One hundred synaptic stimuli (2 Hz) were paired with depolarization (0 mV) where indicated. (Insets) Representative responses obtained before and after LTP induction. Scale bar, 0.3 mV, 10 ms for top traces; 20 pA, 10 ms for bottom traces. (**B**) Expression of GluR1-GFP in pyramidal cells 2 days after infection, imaged with TPLSM. Scale bar, 20 μm. (**C** and **D**) Apical dendrite of CA1 pyramidal cells expressing either GluR1-GFP (C, top and bottom) or plain GFP (D, top and bottom). Scale bar, 5 μm. (**E**) Immuno-electron microscopic image of dendrite expressing GluR1-GFP. Postembedding immunolabeling was performed with antibody to GFP (*18*–*20*). Immunogold particles were mainly distributed inside dendrite. Scale bar, 0.3 μm. (**F**) Distribution of immunogold particles in different dendritic compartments for GluR1-GFP (left) and endogenous GluR1 (right). (Inset) Location of immuno-labeling. See (*20*) for details. (**G**) Surface expression of GluR1-GFP assessed with fluorescent immunostaining. Cells infected with GluR1-GFP were fixed and stained under nonpermeabilized (left) and permeabilized (right) conditions with antibody to GFP (Texas Red detection). Images detected in GFP channel (top) or antibody to GFP channel (bottom). Note immunostaining along dendritic membrane (bottom, left) with no detectable spines. Scale bar, 5 μm.

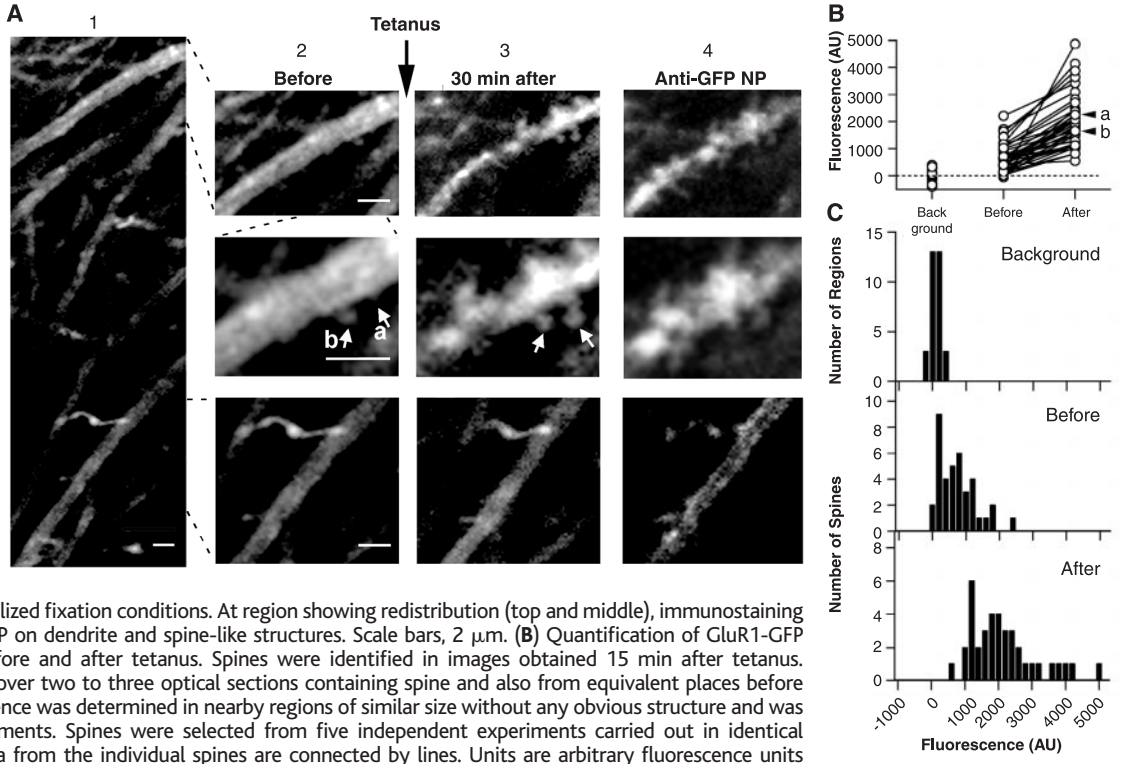

Fig. 4. Tetanic stimulation induces spine delivery and clustering of GluR1-GFP. (**A**) Column 1, GluR1-GFP expression in apical dendritic region. Stimulation electrode was placed in nearby region (~5 to 10 μm from top left corner, outside imaged region). Column 2, region near stimulation electrode (top and middle: two different magnifications of same region) and another region (bottom) imaged before tetanus. a and b denote locations of interest. Column 3, same regions imaged 30 min after tetanic stimulation. Arrows mark regions a and b in column 2. Column 4, surface GluR1-GFP assessed with antibody to GFP immunostaining in nonpermeabilized fixation conditions. At region showing redistribution (top and middle), immunostaining detected increased GluR1-GFP on dendrite and spine-like structures. Scale bars, 2 μm. (**B**) Quantification of GluR1-GFP signal intensity of spines before and after tetanus. Spines were identified in images obtained 15 min after tetanus. Fluorescence was integrated over two to three optical sections containing spine and also from equivalent places before tetanus. Background fluorescence was determined in nearby regions of similar size without any obvious structure and was subtracted from all measurements. Spines were selected from five independent experiments carried out in identical experimental conditions. Data from the individual spines are connected by lines. Units are arbitrary fluorescence units (AU). Imaging parameters were identical before and after tetanus. (**C**) The same data plotted as histograms. Bin width, 200 AU.

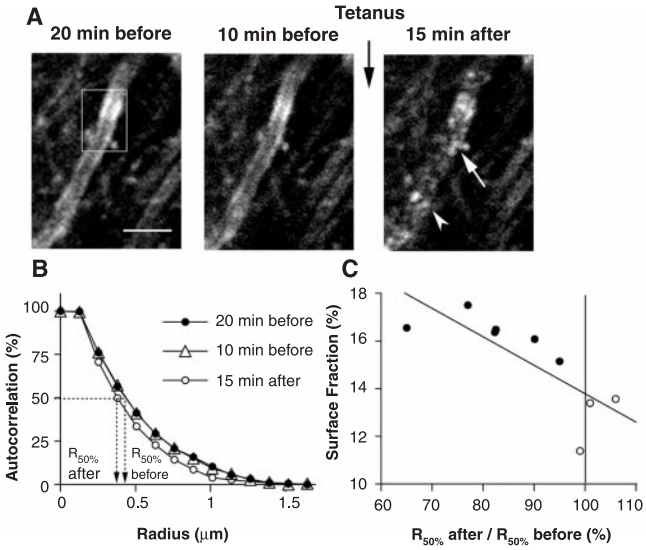

Fig. 5. Tetanic stimulation induces clustering of GluR1-GFP. (**A**) TPLSM images of dendrite before (20 min, left; 10 min, middle) and after (right) tetanic stimulation. Note marked clustering of signal in dendrite, including at the base of a spine (arrow) and at regions without obvious spines (arrowhead). In this example, spine (arrow) became only slightly brighter (10% increase in fluorescence) and no other spines emerged. Scale bar, 2 μm. (**B**) Autocorrelation function computed over boxed region in (A) at 20 min (●) and 10 min (△) before and 15 min after (○) stimulation (*25*). Distance at which function decays to 50% ($R_{50\%}$) was used as a measure of clustering. A decrease in $R_{50\%}$ value indicates cluster formation. (**C**) Dendrites with clustering have more surface GluR1-GFP. Images were taken before and after tetanic stimulation and after immunostaining with antibody to GFP under nonpermeabilized fixation condition. Amount of GluR1-GFP on surface versus total amount of GluR1-GFP is plotted against the ratio of $R_{50\%}$ value before and after the tetanus for dendritic segments that appeared (●) or did not appear (○) to show clustering. A larger value for anti-GFP/GFP ratio indicates that more tagged receptor reached the surface of membrane. A decrease in $R_{50\%}$ value (indicating clustering) is correlated with a larger anti-GFP/GFP ratio ($R = -0.78$; $P < 0.01$).

could be seen at the base of a spine (Fig. 5A, arrow) or with no detectable delivery to spines (Fig. 5A, arrowhead). Clustering was quantified by computing an index of an autocorrelation function ($R_{50\%}$) calculated over a region of interest before and after tetanus (Fig. 5B) (*25*). In the absence of stimulation, this index changed little over time, on average increasing 5.4 ± 6.6% (mean ± SD, N = 20, randomly chosen dendrites) between two observation periods separated by 15 min. However, upon tetanic stimulation, 27 dendritic segments from 18 experiments became clustered ($R_{50\%}$ decreased by 17.8 ± 1.6%, mean ± SD) (*26*). Dendritic regions showing spine delivery of GluR1-GFP generally showed clustering of receptor ($R_{50\%}$ decreased by 18.3 ± 2.6% at the 10 dendrites analyzed above, showing delivery of GluR1-GFP to spines after tetanus).

We wished to determine if tetanus-induced redistribution of GluR1-GFP included delivery to the surface. We first established a method using TPLSM to image surface recombinant receptor in fixed slices (Fig. 3G) (*14*). The distribution and quantification of GluR1-GFP with these methods (13.3 ± 0.9% on surface) generally agree with values obtained with immuno-gold electron microscopy (9% on surface, Fig. 3F). Regions examined in live tissue during stimulation were analyzed for surface distribution after fixation. Regions in which GluR1-GFP had undergone clustering with tetanic stimulation showed a greater amount of receptor at the surface (Figs. 4A, column 4, and 5C; 18.6 ± 0.2 % on surface), although most of the receptor still remained intracellular. At spines that showed GluR1-GFP delivery after a tetanus (including previously "empty spines"), surface GluR1-GFP could also be detected (Fig. 4A). This indicates that some of the GluR1-GFP delivered into spines after a tetanus reached the spine surface, suggesting their contribution to an increase in synaptic transmission.

To determine whether the redistribution of GluR1-GFP by tetanic stimulation requires synaptic activation of NMDA receptors, we conducted experiments with (D,L)-2-amino-5-phosphono valeric acid (APV), a reversible NMDA receptor antagonist (Fig. 6). With APV in the bath, tetanic stimulation produced no clear redistribution of GluR1-GFP (neither spine delivery nor clustering; Fig. 6A). After washing APV for 45 min, another tetanus was delivered at the same site. Now spine delivery and clustering could be detected (see Fig. 6, no APV, −7 and 15 min). Ensemble averages from several experiments in which spine delivery and clustering were monitored in the presence and subsequent absence of APV are shown in Fig. 6B. These results show that both clustering and spine delivery of GluR1-GFP require synaptic activation of NMDA receptors. These experiments also demonstrate that the effect of tetanic stimulation is not due to direct depolarization of dendrites by the current passed through the stimulating electrode, because such effects would not be blocked by APV.

In this study, we showed that the GFP-tagged GluR1 receptor is electrophysiologically functional and mimics a number of cell-targeting properties of endogenous receptors. In dissociated neurons, the protein is delivered to synapses in the absence of evoked activity. In contrast, in slices given no stimulation, a large fraction of the recombinant GluR1-GFP, as well as endogenous GluR1, is found in the intracellular dendritic compartment and excluded from synapses. This difference may explain the observed difficulty with which LTP is generated in dissociated neurons (*27*). This intracellular pool is within 1 to 2 μm of synapses and thus could be rapidly delivered to synaptic sites during plasticity.

Indeed, we found that GFP-tagged receptors in hippocampal slice neurons were rapidly recruited to dendritic spines after a tetanic stimulus (Figs. 4 and 6). Immunostaining indicated that at least some of the recruited GluR1-GFP reached the spine surface. The delivery to the dendritic shaft surface may also represent synaptic delivery, as shaft synapses (or short "stubby" spines) are more common in young tissue (*28*). The spine delivery of the tagged AMPA receptor required synaptic NMDA receptor activation, providing a strong link between receptor recruitment and activity-induced forms of plasticity. These results provide direct evidence showing rapid effects of synaptic activity on postsynaptic membrane trafficking.

In about half of the spines detected with GluR1-GFP after tetanus, there was no fluorescence at the corresponding region before tetanic stimulation. On the basis of their length (0.95 ± 0.17 μm) and a previous study (*29*), these spines are not likely to have been generated after tetanic stimulation. Our previous study indicated that tetanic stimuli do not generate short spines, but rather such stimuli generate filopodial structures that are typically >3 μm in length (*29*). In view of these observations, it is likely that GluR1-GFP was delivered to existing spines and not newly formed spines, although such a possibility cannot be excluded by our results. If receptors were delivered to existing "empty" spines, these could represent "silent synapses": synapses with only NMDA receptors that gain AMPA receptors during LTP (*3*).

Our results build on a number of studies suggesting that the delivery of AMPA receptors to synapses contributes to activity-dependent plasticity. Inhibition of membrane fusion processes in the postsynaptic cell blocks LTP (*30*). Furthermore, the COOH-termini of AMPA receptor subunits GluR2 and GluR4c

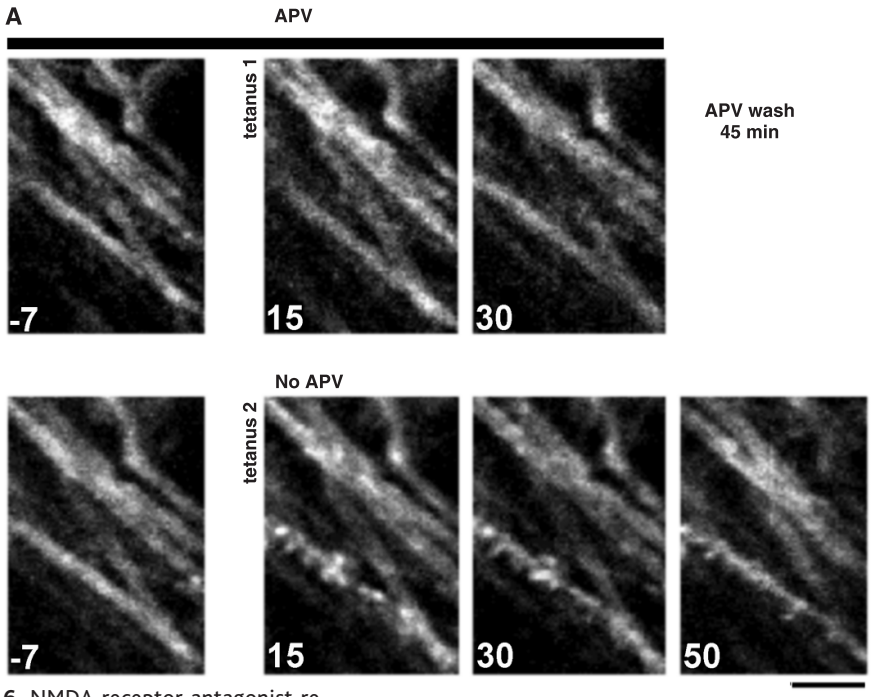

Fig. 6. NMDA receptor antagonist reversibly blocks tetanus-induced redistribution of GluR1-GFP. (**A**) Images of apical dendritic segments obtained at different times during experimental period. (Top) In the presence of 100 μM D,L-APV, tetanus produces little change in fluorescence pattern. (Bottom) After 45 min of drug wash, tetanus at the same site produces both delivery to spines and clustering of GluR1-GFP. In this example, spine delivery persisted at 50 min after tetanus in only two of five spines and clustering reverted to smooth distribution. Time stamps are in minutes relative to tetanus. Scale bar, 5 μm. (**B**) Ensemble averages from experiments carried out as in (A). (Left) Spines showing increased GluR1-GFP fluorescence after tetanus in no APV (tetanus 2) were measured before and after tetanus in APV (tetanus 1). $N = 12$ spines from four experiments. For details of quantification, see legend to Fig. 4B. (Right) Dendritic regions showing clustering in no APV (tetanus 2) were measured before and after tetanus in APV (tetanus 1). $N = 7$ dendrites from seven experiments. For details of quantification, see (*25*).

bind *N*-ethylmaleimide–sensitive fusion protein, a protein involved in membrane fusion processes (*31*). Vesicular organelles, possibly undergoing exocytosis and endocytosis, have been detected with electron microcopy in spines (*32*). And last, dendrites can display a calcium-evoked exocytosis of trans-Golgi–derived organelles that is mediated by the calcium/calmodulin-dependent protein kinase II, an enzyme thought to mediate LTP (*33*). Other postsynaptic mechanisms, such as an increase in conductance of AMPA receptors (*4*, *5*), may also occur in parallel. Our results also do not rule out a contribution by presynaptic modifications.

In addition to the spine delivery of GluR1-GFP, tetanic stimulation induced the formation of clusters of the tagged receptor within dendrites. These structures may be related to the spine apparatus, membranous structures at the base of spines (*32*) that appear to contain AMPA receptors (*34*). The entry of calcium through synaptic NMDA receptors may cause nucleation of AMPA receptor–containing membranes close to active synapses. Once formed, such sites may serve several functions. These sites may replenish those receptors delivered to spines during plasticity. Additionally, they may serve as a "synaptic tag" (*35*), providing a docking site for AMPA receptors synthesized at distant sites. Last, they could provide a site for local AMPA receptor synthesis (*36*). In these capacities, such clusters could represent a structural modification serving as a long-lasting memory mechanism.

References and Notes

1. T. V. P. Bliss and G. L. Collingridge, *Nature* **361**, 31 (1993).
2. D. Muller and G. Lynch, *Proc. Natl. Acad. Sci. U.S.A.* **85**, 9346 (1988); J. A. Kauer *et al.*, *Neuron* **1**, 911 (1988); S. N. Davies *et al.*, *Nature* **338**, 500 (1989).
3. D. Liao *et al.*, *Nature* **375**, 400 (1995); J. T. R. Isaac *et al.*, *Neuron* **15**, 427 (1995); G. Durand *et al.*, *Nature* **381**, 71 (1996); Y. Ben-Ari *et al.*, *Trends Neurosci.* **20**, 523 (1997).
4. T. A. Benke *et al.*, *Nature* **393**, 793 (1998).
5. K. W. Roche *et al.*, *Neuron* **16**, 1179 (1996); Y. Hayashi *et al.*, *Mol. Brain Res.* **46**, 338 (1997); A. Barria *et al.*, *Science* **276**, 2042 (1997); V. Derkach *et al.*, *Proc. Natl. Acad. Sci. U.S.A.* **96**, 3269 (1999).
6. R. S. Petralia *et al.*, *Nature Neurosci.* **2**, 31 (1999).
7. M. Hollmann and S. Heinemann, *Annu. Rev. Neurosci.* **17**, 31 (1994).
8. R. J. Wenthold *et al.*, *J. Neurosci.* **16**, 1982 (1996).
9. GFP (enhanced GFP; Clontech) was inserted between the third and fourth amino acids after the predicted signal peptide cleavage site of rat GluR1-flop cDNA with standard molecular biology techniques. HEK cells were transfected with plasmid-based mammalian expression vector with lipofectin (Gibco-BRL Life Technologies). GluR1-GFP and GluR2 were cotransfected in 1:4 ratio. Protein immunoblotting was carried out with antibodies to GluR1 COOH-terminal (0.1 μg/ml; Chemicon International). Whole-cell recordings were obtained 2 to 5 days after transfection in Hepes (10 mM)-buffered Hanks' solution in the presence of 100 μM cyclothiazide. Kainate (1 mM) was applied through a puffer pipette positioned close to recorded cell. Five to ten records were obtained at holding potentials of −80 to 60 mV (20-mV steps).
10. I. Frolov *et al.*, *Proc. Natl. Acad. Sci. U.S.A.* **93**, 11371 (1996); R. Malinow *et al.*, in *Imaging Living Cells* (Cold Spring Harbor Laboratory Press, Cold Spring Harbor, New York, in press).
11. Whole-cell recordings from neurons infected with Sindbis virus for 1 to 4 days show normal passive membrane properties (for example, input resistance: uninfected, 276 ± 64, $N = 13$; GluR1-GFP infected, 302 ± 51, $N = 8$; $P = 0.78$) (S. Shi, Y. Hayashi, R. Malinow, unpublished results).
12. Dissociated cultured neurons were prepared as previously described (*33*).
13. To estimate the level of recombinant GluR1-GFP expression, relative to endogenous GluR1 expression, we performed immunohistochemistry on fixed (*14*) dissociated hippocampal neurons (*33*) with a GluR1 COOH-terminal antibody (1 μg/ml; Chemicon International) that recognizes both proteins (Fig. 1B) as primary and Texas Red coupled as secondary (which does not overlap in fluorescence with GFP). In a field of infected and noninfected cells, dendrites (80 μm from cell body) of infected cells showed 2.7 ± 0.2 fold (mean ± SEM, $N = 8$) immunolabel compared with similar regions of uninfected cells.
14. Tissue was fixed with freshly made 4% paraformaldehyde and 4% sucrose in phosphate-buffered saline (PBS) (dissociated neurons: 4°C for 30 min; organotypic slices (*16*): 4°C for 1 hour). With such fixation, immunohistochemistry (see below) detected only surface epitopes (dissociated cells: Fig. 2C; organotypic slices: Fig. 3G). To detect intracellular epitopes, tissue was further treated with 0.3% Triton X-100 in PBS (dissociated cells: 4°C for 10 min; organotypic slices: 4°C for 30 min). Immunohistochemistry: Cells were blocked in blocking solution (10% horse serum in PBS; 60 min) and then incubated with primary antibody (4°C, overnight) in blocking solution. All primary rabbit polyclonal antibodies were visualized with biotin-conjugated antibody to rabbit immunoglobulin G (IgG) and Texas Red–avidin system. Mouse monoclonal antibodies were visualized with antibodies to mouse IgG labeled with Cy5 (Jackson ImmuoResearch). Images of dissociated neurons were collected with a cooled charge-coupled device (Photometrics) and analyzed with PMIS or V for Windows (Photometrics); organotypic slices were imaged with TPLSM (*21*). Fraction of GluR1-GFP molecules on surface for a given region can be quantified by computing [(antibody to GFP signal)/(GFP signal)] in nonpermeabilized conditions for that region and normalizing by [(antibody to GFP signal)/(GFP signal)] obtained from similar tissue in permeabilized conditions. Signals in above computation indicate background subtracted values.
15. For whole-cell recordings from dissociated neurons, internal solution consisted of (in mM) 115 cesium methanesulfonate, 20 CsCl, 10 Hepes, 2.5 $MgCl_2$, 4 Na_2-adenosine triphosphate, 0.4 Na-guanosine triphos-

phate, 10 Na-phosphocreatine, and 0.6 EGTA (pH 7.2). Neurons were perfused with artificial cerebrospinal fluid (ACSF) of the following composition (in mM): 119 NaCl, 2.5 KCl, 4 $CaCl_2$, 4 $MgCl_2$, 26.2 $NaHCO_3$, 1 NaH_2PO_4, and 11 glucose; then the neurons were gassed with 5% CO_2 and 95% O_2 at 28°C. Responses to glutamate were evoked by adding (in μM) 40 L-glutamic acid γ-(α-carboxyl-2-nitrobenzyl) ester (Molecular Probes), 1 tetrodotoxin, 100 picrotoxin, 100 APV, and 1 3-((R)-2-carboxypiperazin-4-yl)-propyl-1-phosphoric acid. Ten to 25 ms of flash (100 W of Hg; quartz optics, Zeiss Axiovert 135) was delivered to a spot (~50-μm diameter) positioned over dendrites.

16. Organotypic slice culture of hippocampus was prepared as described [L. Stoppini *et al*., *J. Neurosci. Methods* **37**, 173 (1991)]. Hippocampal slices (400 μm) were cut from postnatal 6- to 8-day-old rats with tissue chopper and cultured in medium as described [W. Musleh *et al*., *Proc. Natl. Acad. Sci. U.S.A.* **94**, 9451 (1997)]. Slices were placed in a recording chamber and perfused with ACSF. Synaptic transmission was evoked (0.1 Hz, 100 μs, ~10 V) with a glass stimulation electrode (1 to 2 megaohms, filled with 3 M NaCl), positioned in CA1 stratum radiatum. Tetanic stimuli consisted of two 100-Hz trains of 1-s duration separated by 20 s.
17. D. L. Pettit *et al*., *Science* **266**, 1881 (1994).
18. R. S. Petralia *et al*., *J. Comp. Neurol.* **385**, 456 (1997).
19. A. Miyawaki *et al*., *Nature* **388**, 882 (1997).
20. The distribution of GluR1 and GluR1-GFP was measured quantitatively with immuno-gold labeling (*18*). Sections from dendritic regions ~100 μm from the cell bodies were examined. To identify a cell infected with GluR1-GFP virus, we identified a dendritic segment (~1 μm in diameter) with immunolabeling. Comparable regions (with dendritic segments ~1 μm in diameter) were chosen in tissue from uninfected P10 animals for analysis of endogenous GluR1. For each section, the label was identified as being in one of the following compartments: A, dendritic cytosol; B, dendritic surface; C, spine, non-PSD; and D, PSD. The total number of grains counted was 515 for endogenous GluR1 and 785 for GluR1-GFP. For background subtraction, 50 presynaptic terminals were randomly chosen, label was counted, and density was calculated (0.17 gold per square micrometer). This background density constituted 10 to 20% of the signal found in dendritic cytosol (0.92 gold per square micrometer) and was subtracted to reach dendritic cytosol value (A, above); this region is the only compartment with sufficient area to be affected by background labeling.
21. K. Svoboda *et al*., *Science* **272**, 716 (1996); W. Denk and K. Svoboda, *Neuron* **18**, 351 (1997); Z. F. Mainen *et al*., *Methods*, in press. Optical stacks (30 μm by 30 μm by 50 μm; step size, 0.5 μm) were captured about every 15 min with a custom-built two-photon laser scanning microscope [Zeiss, 63X objective; Ti: sapphire laser tuned to wavelength (λ) ~ 900 nm]. Stimulation electrode was placed nearby dendrites expressing GluR1-GFP under visual guidance. Quantification of fluorescence from images was carried out with custom-made programs in IDL (Research Systems). Images were imported into Adobe Photoshop for figure presentation. Each displayed image is generally the average of three to five optical sections. In some cases, an image is the composite of images captured at slightly different (~1 μm) optical sections; this was necessary to offset tilting of structures over the course of hours of examination.
22. Single-spine Ca^{2+} imaging studies with the same stimulus electrodes (tip resistance, 1 to 2 megaohms) and parameters indicate that synaptic excitation in this preparation is sparse. Thus, as in previous studies (*21*, *37*), the tip of the stimulating electrode must be placed around 5 to 15 μm from imaged postsynaptic regions.
23. Within 3 SD of the noise measured in background regions.
24. The random fluctuation of GluR1-GFP fluorescence was measured in six spines identified during control conditions. At these spines, the GluR1-GFP intensity decreased 344 ± 259 AU (mean ± SD) from one observation period to the next (from 1755 ± 613 AU to 1411 ± 478 AU). Thus, the increase in spine GluR1-GFP fluorescence after tetanus differs (by 6 SD for "active" spines and by 7 SD for "empty" spines) from the average changes seen in the absence of tetanus. This indicates that such events are unlikely to occur from chance alone. Furthermore, the density of GluR1-GFP–containing spines detected after tetanus in the analyzed dendrites (0.93 ± 0.12 μm^{-1} over 10 dendritic segments 7.5 ± 4.7 μm in length) was ~16 SD outside the mean density of GluR1-GFP–containing spines detected in the absence of tetanus (0.021 ± 0.055 μm^{-1}, mean ± SD, measured over 30 randomly chosen dendritic segments).
25. After selecting a region of interest (about 8 μm by 8 μm by 3 μm), an autocorrelation function, $A(r)$, of fluorescence intensity, $I(x, y, z)$, was computed as a function of distance, r:

$$A(r) = \Sigma_x\Sigma_y\Sigma_z\Sigma_{\theta r}[I(x, y, z)*I(x_{\theta r}, y_{\theta r}, z)]/$$
$$[I(x, y, x) + I(x_{\theta r}, y_{\theta r}, z)]^2$$

where θr indexes x and y over 72 locations about a circle centered at x, y and of radius r. This function decayed smoothly and monotonically as a function of distance (Fig. 5B), reflecting the nonperiodic distribution of fluorescence. We used the distance at which the autocorrelation function reached 50% decay ($R_{50\%}$) as an index of signal homogeneity.
26. This decrease is 3.6 SD beyond those changes seen in the absence of stimulation, indicating a small likelihood that these changes occur from chance alone.
27. J. M. Bekkers and C. F. Stevens, *Nature* **346**, 724 (1990).
28. K. Harris *et al*., *J. Neurosci.* **12**, 2685 (1992).
29. M. Maletic-Savatic *et al*., *Science* **283**, 1923 (1999).
30. P.-M. Lledo *et al*., *ibid.* **279**, 399 (1998).
31. A. Nishimune *et al.*, *Neuron* **21**, 87 (1998); P. Osten *et al.*, *ibid.*, p. 99; I. Song *et al.*, *ibid.*, p. 393.
32. J. Spacek and K. M. Harris, *J. Neurosci.* **17**, 190 (1997).
33. M. Maletic-Savatic and R. Malinow, *ibid.* **18**, 6803 (1998); M. Maletic-Savatic *et al*., *ibid.*, p. 6814.
34. Z. Nusser *et al.*, *Neuron* **21**, 545 (1998).
35. U. Frey and R. G. Morris, *Nature* **385**, 533 (1997).
36. P. Worley, *Neuron* **21**, 936 (1998).
37. R. Malinow *et al*., *Proc. Natl. Acad. Sci. U.S.A.* **91**, 8170 (1994); R. Yuste and W. Denk, *Nature* **375**, 682 (1995); H. Takechi *et al*., *ibid.* **396**, 757 (1998).
38. We thank S. Schlesinger for Sindbis virus expression system; P. De Camilli for antibody against synapsin I; C. S. Zucker for antibody to GFP; J. Boulter, S. F. Heinemann, and P. H. Seeburg for cDNA clones; N. Dawkins-Pisani, B. Burbach, and P. O'Brian for technical assistance; and Y.-X. Wang for assistance in the immunogold studies. Y.H. is a recipient of research fellowships from Japan Society for the Promotion of Science and Uehara Memorial Foundation. S.H.Z. was a recipient of Wellcome Trust Fellowship. This study was supported by the NIH (R.M. and K.S.), the Mathers Foundation (R.M.), and the Human Frontier Science Program, Pew, and Whitaker Foundations (K.S).

1 February 1999; accepted 4 May 1999

REPORTS

Reconstructing Phylogeny with and without Temporal Data

David L. Fox,* Daniel C. Fisher, Lindsey R. Leighton

Conventional cladistic methods of inferring evolutionary relationships exclude temporal data from the initial search for optimal hypotheses, but stratocladistics includes such data. A comparison of the ability of these methods to recover known, simulated evolutionary histories given the same, evolved character data shows that stratocladistics recovers the true phylogeny in over twice as many cases as cladistics (42 versus 18 percent). The comparison involved 550 unique taxon-by-character matrices, representing 15 evolutionary models and fossil records ranging from 100 to 10 percent complete.

Phylogenetic analysis seeks to identify the pattern of historical relationships among organisms. However, controversy persists over not only what constitutes an appropriate inference strategy, but also what categories of data are acceptable as evidence (*1*). One recent debate focuses on the use of stratigraphic data, or the temporal order of specimens in the fossil record, as evidence for inferring relationships (*2*). Proponents of cladistic methods often argue that temporal data may be misleading as indicators of relationship (*3*). Arguments supporting this position are essentially a priori and do not address the relative efficacy of methods that do and do not use temporal data. We explore the efficacy of using temporal data through simulations of evolutionary histories and associated character data, assessing the relative performance of two phylogenetic methods, cladistics and stratocladistics.

Both conventional cladistic analysis and stratocladistics rely on parsimony, in the sense of minimizing ad hoc auxiliary hypotheses, to evaluate alternative interpretations of relationship. Cladistic analysis selects interpretations that minimize hypotheses of homoplasy, or shared traits that do not result from common ancestry (*4*, *5*). Hypotheses of homoplasy are counted individually and, lacking contravening evidence, equally.

Stratocladistics (*6*) incorporates stratigraphic data into the logic of cladistic hypothesis choice by selecting interpretations of relationship that minimize hypotheses of homoplasy and nonpreservation of lineages through intervals that preserve other lineages under analysis, giving neither category of